NeuroImage 334 (2026) 121957

Contents lists available at ScienceDirect

NeuroImage

journal homepage: www.elsevier.com/locate/ynimg

Exploratory decoding of TMS–EEG: Predicting TEP response to intermittent and continuous theta burst stimulation

Arne Callaert [a,*], Kristl Vonck [b], Diego Nieves Avendaño [a], Sofie Carrette [b], Chiara Silvestri [b], Philipp Schnepel [c], Vojkan Mihajlović [c], Evelien Carrette [b,1], Femke Ongenae [a,1], Sofie Van Hoecke [a,1]

[a] IDLab, Department of Electronics and Information Systems, Ghent University–imec, Ghent, Belgium
[b] 4BRAIN, Institute for Neuroscience, Department of Neurology, Ghent University, Ghent, Belgium
[c] Imec Netherlands, Eindhoven, The Netherlands

ARTICLE INFO

Keywords:
Transcranial magnetic stimulation (TMS)
TMS–EEG
Intermittent and continuous theta burst stimulation (iTBS and cTBS)
TMS-evoked potential (TEP)
Resting-state EEG (rEEG)
Machine learning (ML)

ABSTRACT

Theta burst stimulation (TBS) is a promising form of repetitive transcranial magnetic stimulation (rTMS) capable of modulating cortical excitability and intracortical processes, offering therapeutic potential for neurological and psychiatric disorders. However, clinical translation remains limited by high inter-subject and inter-session variability in stimulation effects. To more directly capture cortical responses, there is increased interest in combining TMS with electroencephalography (EEG) to assess TMS-evoked potentials (TEPs) before and after stimulation. As an individual's neurophysiological state influences stimulation outcomes, this study explores whether pre-stimulation resting-state EEG can predict changes in TEP component amplitudes following intermittent (iTBS) and continuous (cTBS) protocols applied to the left primary motor cortex, using data from fifteen healthy male participants in a randomized, single-blind crossover design. Linear (Lasso regression) and nonlinear (CatBoost regression) models were designed to predict changes in six TEP components (N15, P30, N45, P60, N100, P180). Both models consistently achieved lower mean absolute errors than the random guessing baseline, demonstrating their ability to capture meaningful predictive patterns in cortical responses. The best performing model varied by TEP component and TBS protocol. Incorporating feature deltas (post- vs. pre-stimulation feature difference) did not significantly enhance predictive performance. Feature importance analysis revealed the predictive value of spectral power and connectivity measures. For instance, connectivity between the stimulation site and frontal/parietal regions, together with oscillatory power in frontal and motor areas, often emerged as the top predictors. Given the limited sample size, these findings should be interpreted as exploratory and hypothesis-generating, requiring validation in larger and independent cohorts. The study establishes a framework for predicting individual TEP responses to TBS using machine learning, paving the way for personalized neuromodulation.

1. Introduction

Transcranial magnetic stimulation (TMS) is a non-invasive brain stimulation (NIBS) technique that uses rapidly changing magnetic fields to induce electrical currents in the brain's cortex through electromagnetic induction. A specific form of repetitive TMS (rTMS), known as theta burst stimulation (TBS), delivers short bursts of three high-frequency (50 Hz) pulses at a theta rhythm (5 Hz). TBS is considered a promising neuromodulation technique due to its ability to modulate cortical excitability with relatively short stimulation durations and low intensities (Chung et al., 2015, 2016), while producing neuroplastic effects comparable to or greater than conventional rTMS (Huang et al., 2005). TBS has demonstrated therapeutic potential in treating youth with Major Depressive Disorder (MDD) who are unresponsive to traditional therapies (Dhami et al., 2019), and it is increasingly being investigated for a broader range of neurological and psychiatric disorders (Zhang et al., 2023; Cole et al., 2024).

TBS is commonly delivered in two paradigms: continuous TBS (cTBS), where bursts are applied without interruption, and intermittent TBS (iTBS), where a 2-second burst is followed by an 8-second rest period. When applied to the primary motor cortex (M1), cTBS has

* Corresponding author.
E-mail address: arne.callaert@ugent.be (A. Callaert).
[1] Contributed equally as senior authors and jointly supervised this work.

https://doi.org/10.1016/j.neuroimage.2026.121957
Received 5 January 2026; Received in revised form 7 April 2026; Accepted 27 April 2026
Available online 29 April 2026

been linked to long-term depression (LTD)-like effects, while iTBS has been associated with long-term potentiation (LTP)-like effects (Suppa et al., 2016; Huang et al., 2017). While these are often referred to as "inhibitory" and "excitatory" paradigms, this binary classification may oversimplify the underlying TBS-induced neurophysiological modulation. In practice, responses vary substantially across individuals, with some even exhibiting opposite effects, thereby challenging the reliability of this classification (Carrette et al., 2025; Rocchi et al., 2018).

The variability of TBS-induced effects between individuals (inter-subject variability) and within the same individual across sessions (intra-subject variability) poses a significant challenge to its clinical adoption as a reliable neuromodulation tool (Terranova et al., 2019). The variability can arise from a combination of intrinsic neurophysiological factors (e.g., neurophysiological brain state, cortical and spinal excitability, synaptic plasticity, anatomy, age, gender, time of day) as well as stimulation delivery factors (e.g., stimulation parameters, orientation, and coil positioning) (Huang et al., 2017; Rocchi et al., 2018). Further variability may be introduced at the level of effect characterization, depending on data preprocessing choices, the analysis pipeline, and the selected measures used to quantify the induced effects.

When applied to the motor cortex, the effects of TMS can be indirectly assessed by recording motor outputs from peripheral muscles controlled by the stimulated cortical region using surface electromyography (EMG). This yields compound motor-evoked potentials (MEPs), which provide a simple and immediate measure of TBS-induced effects (McCalley et al., 2021). Changes in MEP amplitudes are often used as a proxy for motor cortical excitability and to classify individuals as responders or non-responders based on whether MEPs increase or decrease relative to baseline (Huang et al., 2017; Katagiri et al., 2024). However, MEPs are inherently variable and influenced by factors such as muscle state (e.g., resting vs. active) and the balance of excitatory and inhibitory neural circuits (Wassermann et al., 2008). Moreover, MEPs provide only an indirect measure of cortical excitability, reflecting the excitability of a subpopulation of output neurons that project to the spinal cord (i.e., corticospinal excitability), and therefore fail to capture the full complexity of intracortical processes and cortical excitability (Rocchi et al., 2018; Ozdemir et al., 2021).

To address limitations of MEPs as a proxy, there has been growing interest in the co-registration of TMS with electroencephalography (TMS-EEG), which enables direct measurement of cortical responses with high temporal resolution and broad spatial coverage (Farzan and Bortoletto, 2022). TMS-evoked potentials (TEPs), derived from EEG signals phase-locked to single-pulse TMS, offer a more nuanced and temporally precise measure of cortical reactivity, excitability, connectivity, and neuroplastic changes compared to MEPs (Speranza et al., 2024; Rocchi et al., 2018). TEPs are defined by distinct waveform components, marked by a series of negative (N) and positive (P) voltage deflections at specific latencies (ms), including N15, P30, N45, P60, N100, and P180. These negative and positive amplitude peaks, referred to as components, are thought to reflect a combination of excitatory and inhibitory cortical processes within neuronal populations, activated directly by TMS or indirectly through a combination of cortico-subcortical and cortico-cortical network interactions (Rogasch and Fitzgerald, 2013; Carrette et al., 2025). Pharmacological TMS–EEG studies suggest that certain TEP components show sensitivity to GABAergic neurotransmission. For example, the N45 has been associated with $GABA_A$-mediated inhibitory processes, while the N100 has been associated with $GABA_B$-related inhibition (Premoli et al., 2014). However, the functional specificity and precise mechanisms underlying these components remain an active area of research.

While TEPs are considered direct and reproducible measures of cortical responsivity (Hernandez-Pavon et al., 2023), they are more challenging to process than MEPs due to several potential confounders. Early components (e.g., N15) may be contaminated by cranial muscle activity, while later components (e.g., N100, P180) can be influenced by sensory-evoked responses to the TMS pulse, such as the coil click or somatosensory scalp sensations (Hernandez-Pavon et al., 2023). In addition, the TMS pulse induces a strong electromagnetic artifact in the EEG leads, typically restricted to the first 10 ms post-pulse. Despite these challenges, TEP attributes, such as amplitude, latency, and scalp distribution, provide valuable insights into the strength and nature of TMS-evoked cortical responses, offering a more direct and nuanced reflection of the induced effect.

Given the growing evidence that neurophysiological differences, such as ongoing dynamics and cortical excitability levels, influence TBS outcomes, this study investigates whether the brain's resting-state dynamics, as captured by pre-stimulation resting-state EEG (rsEEG), can be used to predict responsiveness to TBS by predicting individual changes in TEP components following iTBS and cTBS. Given the high dimensionality of EEG signals and the complexity of feature interaction, machine learning (ML) approaches present a promising methodology for identifying predictive patterns. Advances in ML offer new opportunities for predicting and understanding individual responses to neuromodulation. Previous studies have highlighted the importance of identifying neurophysiological markers for TBS outcomes and the potential of ML to achieve this (Dhami et al., 2023; Katagiri et al., 2024; Cai et al., 2024). However, these works either used motor-evoked potentials (MEPs) as the outcome measure (Dhami et al., 2023; Katagiri et al., 2024) or relied on simple feature-outcome associations (Cai et al., 2024). In contrast, our study is the first to employ ML to predict changes in TEP components directly.

We therefore designed and evaluated two predictive models, a linear model (Lasso) and a nonlinear model (CatBoost), to predict the amplitude changes of all six TEP components mentioned earlier. In addition, the study investigated whether including post-stimulation rsEEG information, by supplying the model with the change in feature values (delta), could enhance predictive performance. Finally, we analyzed the models to identify predictive features that could serve as potential biomarkers for responsiveness.

Predicting individual cortical responses before stimulation (e.g., whether the N45 amplitude will increase after cTBS) would represent a valuable step toward personalized TBS. Such predictions could guide clinical decisions, for example, by postponing or withholding stimulation if no beneficial response is expected, or by adapting stimulation parameters (e.g., intensity or number of pulses). By improving our ability to predict and tailor neuromodulation effects to each individual's brain, we may reduce variability in TBS outcomes and support the development of individualized therapeutic strategies for psychiatric and neurological disorders.

The remainder of this paper is organized as follows. Section 2 describes the experimental design, stimulation protocol, and preprocessing pipeline for both the rsEEG and TMS-EEG recordings. The ML approach, including feature extraction, model design and evaluation strategies, is also introduced. Section 3 presents the predictive performance of both the linear and nonlinear model across TEP components and stimulation protocols, followed by a feature importance analysis. Section 4 discusses the implications of the findings and outlines potential limitations. Finally, in Section 5, the main insights are summarized.

2. Materials and methods

2.1. Experimental design and TMS protocol

Fifteen right-handed adult male volunteers were recruited at Ghent University Hospital for this study (Carrette et al., 2025). Participants were screened for TMS contraindications, instructed to limit caffeine intake, and advised to ensure sufficient sleep before each session, to reduce response variability (Guerra et al., 2020). Female participants were excluded to avoid menstrual cycle-related variations in cortical excitability.

Each participant participated in three sessions at least one week apart, following a randomized, crossover design. During each session, either cTBS,iTBS, or sham (active control) was delivered to the left primary motor cortex (M1). Single-pulse TMS-EEG measurements (150 biphasic pulses at 80% of the resting motor threshold (rMT)) were recorded approximately 20–30 min before and within 10 min after TBS. The order of TBS conditions was randomized, and participants were blinded to which condition they received.

TMS sessions were conducted using a MagPro X100 stimulator (MagVenture, Farum, Denmark) equipped with a static-cooled 65-mm figure-of-eight coil. A schematic overview of the experimental procedure per session is illustrated in Fig. 1. The functional motor hotspot (fHS) of the left primary motor cortex (M1) was determined based on optimal responses in the right first dorsal interosseous (FDI) muscle and registered using a neuronavigation system (Localite GmbH, Bonn, Germany) to ensure consistent coil positioning. Stimulation intensity (80% rMT) was determined via an adaptive threshold-hunting method (ML-PEST; MTAT 2.0) (Carrette et al., 2025). TBS followed standard parameters, involving triplets of pulses at 50 Hz every 200 ms (5 Hz). In the cTBS protocol, bursts were delivered continuously for 40 s (600 pulses total). In the iTBS protocol, bursts were delivered for 2 s followed by an 8-second pause, resulting in 190 s of stimulation (600 pulses total). For the active-control condition, a 25-mm plastic spacer was inserted between the coil and the scalp to minimize effective cortical stimulation.

EEG was recorded using 62 scalp electrodes (BrainCap TMS, Brainproducts GmbH, Gilching, Germany) with DC amplifiers (BrainAmp Mrplus, Brainproducts GmbH). Electrode impedances were kept below 5 kΩ, and the signal was digitized at 5 kHz (DC-1000 Hz bandwidth). Reference and ground electrodes were placed on the forehead, and eye movements were monitored with two electrooculogram channels. A recent study suggested that TEP amplitudes could be influenced by the stimulation of peripheral nerves and the loud clicking noise produced by the TMS coil (Conde et al., 2019). Therefore, to minimize TMS-related auditory and somatosensory contributions, participants wore earphones playing masked colored noise (broadband noise that matches the spectral content of the TMS click), and a foam layer was inserted between the coil and the EEG cap to reduce mechanical vibration and scalp sensation. Although such masking does not fully eliminate bone-conducted transmission of the click, it substantially reduces the air-conducted component and the resulting auditory-evoked potential (Rogasch and Fitzgerald, 2013). Single-pulse TMS was kept at subthreshold intensity (80% rMT) to reduce scalp muscle activity and avoid distal MEPs in other muscles. Further, the coil orientation was slightly adjusted, without shifting its center of the hotspot, to limit muscle artifacts.

2.2. TEP preprocessing

The absence of a standardized preprocessing pipeline for TEP has contributed to considerable variability across studies, hindering reproducibility and cross-study comparisons (Brancaccio et al., 2024; Rogasch et al., 2022). A major challenge lies in the lack of ground truth references (a definitive representation of the "clean" signal), which makes it difficult to objectively evaluate the effectiveness of different artifact removal strategies (Bertazzoli et al., 2021). Recent evaluations using synthetic TMS-EEG data have compared different preprocessing pipelines (Brancaccio et al., 2024) and highlighted the robustness and reliability of the TESA toolbox (TMS-EEG Signal Analyzer) (Rogasch et al., 2017), showing lower variability relative to alternatives such as ARTIST (Wu et al., 2018) and SOUND/SSP-SIR (Mutanen et al., 2018, 2016). Additionally, streamlining the preprocessing with TESA across patients for both pre- and post-TEP data ensures better comparability of pre- and post-TBS results and reduces inconsistencies from manual or heterogeneous cleaning methods.

The EEG signals were thus preprocessed using the EEGLAB and TESA Matlab toolboxes (Delorme and Makeig, 2004; Rogasch et al., 2017; Mutanen et al., 2020). First, channels with kurtosis exceeding 3.5 standard deviations (SDs) from the mean were considered noisy and removed (high kurtosis indicates large amplitude deviations). Next, the signal was epoched from −800 ms to 800 ms around each TMS pulse, and baseline correction was applied using the pre-pulse interval between −500 and −15 ms. The electromagnetic pulse artifact, which arose from −4 to 14 ms (through manual inspection), was removed and then interpolated (cubic spline) to maintain signal continuity. Further, the signal was downsampled to 1000 Hz, and noisy epochs were identified and removed using a joint probability criterion to detect data segments whose amplitude distribution deviates from the overall channel distribution by more than 3 standard deviations across channels.

Independent component analysis (ICA) is a blind source separation technique that decomposes EEG into temporally independent components, allowing for the identification and removal of stereotyped artifacts while preserving neural activity (Makeig et al., 1995). An initial (Fast) ICA was performed before bandpass filtering to isolate and remove the large-amplitude, short-latency artifacts that occur immediately after the TMS pulse (e.g. scalp muscle contractions). Removing these broadband artifacts early prevents them from distorting later filtering and improves the separation of neural and artifact sources. The TESA automated component classification and selection method was then used to identify and reject components related to TMS-induced muscle activity. Subsequently, a bandpass filter from 1 to 100 Hz was applied to remove unwanted frequencies and a notch filter between 48 and 52 Hz to eliminate the line noise. The second round of ICA then targeted residual, non-TMS-locked artifacts, such as eye blinks, eye movements, persistent muscle activity, and electrode noise (again using the TESA component labeler). Finally, the previously removed channels were reconstructed using spherical interpolation, and the channels were referenced to the average.

For the pre- and post-repeated single pulse phases, all 150 single pulses (epochs) are averaged to get the TEP response. As the choice of channels influences the TEP waveform, the C3, C1 and Cz channels are selected and averaged due to their proximity to the stimulation site, which was considered the region of interest in this study. Because TEP peak latencies varied across participants and stimulation conditions, amplitudes were extracted using automated peak-detection, whereby the local maximum or minimum was identified within predefined latency windows (N15: 10–20 ms; P30: 20–36 ms; N45: 37–52 ms; P60: 55–65 ms; N100: 75–110 ms; P180: 140–200 ms). Peaks were visually verified, and in some cases where a component of a participant fell just outside the window, the search interval was minimally adjusted to ensure accurate extraction.

2.3. Resting-state EEG preprocessing

The rsEEG data were preprocessed in Python using the MNE library (Gramfort et al., 2013). A bandpass filter (1–100 Hz) and a notch filter at 50 Hz were applied, followed by detrending and downsampling to 1000 Hz. The data were segmented into 2-second epochs. ICA with the extended infomax algorithm was performed, following the recommendations of the automated component labeler (MNE-ICA label) (Li et al., 2022). Electrooculogram (EOG) channels were available and first used to identify components related to eye movements and blinks. Next, the MNE-ICA label method was applied to classify the remaining components. Only components classified as brain activity with a probability higher than 90% according to the model were retained, while others were excluded. Finally, the missing channels were reconstructed using spherical interpolation.

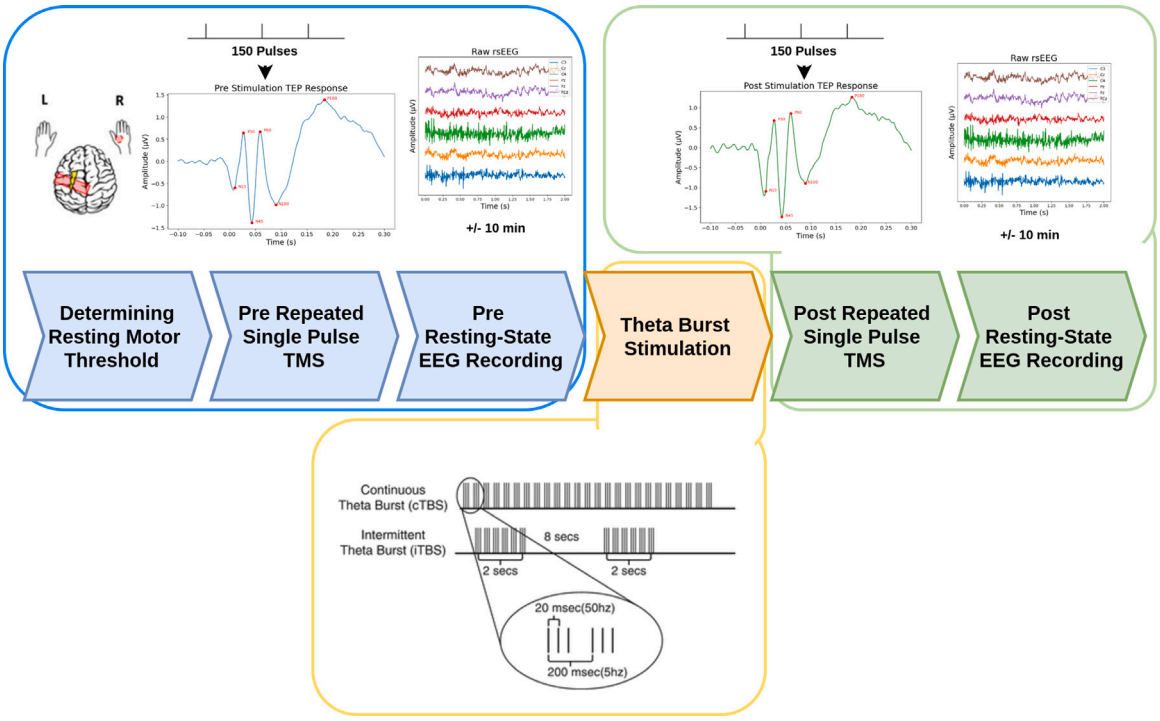

Fig. 1. Schematic overview of the experimental procedure per session. Stimulation was delivered over the left primary motor cortex (M1), targeting the site eliciting the maximal response in the right first dorsal interosseous (FDI) muscle. The stimulation intensity was set at 80% of the resting motor threshold (rMT), which was determined at the start of each session. The session began with 150 single TMS pulses to obtain pre-stimulation TMS-evoked potential (pre-TEP), followed by approximately 10 min of resting-state EEG recording and a 20-minute break. Participants then received either intermittent TBS (iTBS; 2 s of stimulation, 8 s pause, repeated for 190 s) or continuous TBS (cTBS; uninterrupted stimulation for 40 s), both consisting of 600 pulses in total. Immediately after TBS, another 150 single TMS pulses were delivered (post-TEP), followed by a second resting-state EEG recording.

2.4. Feature extraction

TBS is thought to influence cortical excitability through modulation of excitatory and inhibitory neural processes. As noted before, the neurophysiological brain state at the time of stimulation can influence the response to TBS. This highlights the importance of characterizing baseline brain dynamics prior to stimulation as it may influence the response. Therefore, this study designed features from pre-stimulation rsEEG data to quantify this neurophysiological state, focusing on features that are often interpreted as markers of "intrinsic excitability" and connectivity of the brain.

This approach is informed by excitation/inhibition (E/I) balance proxies, which aim to capture the dynamic equilibrium between excitatory and inhibitory neural activity and reflect ongoing fluctuation of synaptic input "at rest" (Pellegrino et al., 2024; Gao et al., 2017). The extracted features are explained below and include the phase locking value (PLV), power spectral density (PSD), sample entropy, and the aperiodic exponent of the PSD. By extracting these features, we aimed to provide the model with patient-specific information that may help predict individual TEP changes.

The ***Phase Locking Value (PLV)*** measures the consistency of phase differences between two signals and is frequently used in functional connectivity analysis to quantify synchronization between different brain regions. PLV reflects the mean spatial phase synchronization and has been shown in high-gamma frequency bands to correlate with cortical excitability, as estimated via perturbational approaches and modulated by antiseizure medications in epilepsy patients (Meisel et al., 2015, 2016).

Given two signals $x(t)$ and $y(t)$, the signals are first band-pass filtered to a frequency range of interest, and the instantaneous phases $\phi_x(t)$ and $\phi_y(t)$ are extracted using the Hilbert transform. The PLV is computed as the modulus of the circular mean of the phase differences over T time points:

$$\mathrm{PLV} = \left| \frac{1}{T} \sum_{t=1}^{T} \exp\left(i\left[\phi_x(t) - \phi_y(t)\right]\right) \right| \quad (1)$$

The circular mean treats phase differences as angles on a unit circle, and the PLV is the magnitude of the average vector formed by these angles. If the phase differences are consistent over time (i.e., $\phi_x(t) - \phi_y(t)$ is constant), the vectors point in the same direction, and their sum will have a magnitude close to 1 (perfect phase locking). If the phase differences are random or spread out, the vectors point in different directions, and their sum cancels out, reducing the magnitude close to 0 (complete absence of phase locking).

In this study, we compute PLV across the following frequency bands: Theta (4–8 Hz), Alpha (8–12 Hz), Low Beta (12–20 Hz), High Beta (20–30 Hz), Low Gamma (30–45 Hz), and High Gamma (55–95 Hz). These bands are associated with distinct neural processes: lower frequencies (Theta and Alpha) are linked to large-scale network coordination and attentional states, while Beta and Gamma bands are more closely related to motor control and cognitive processing.

The aim was to identify potentially relevant connections that may influence TBS response. To this end, PLV was extracted from electrode pairs centered on the stimulation target (left M1 at C3) and its nearest functional partners in frontal/frontocentral (F3, FC3), parietal (P3), central (Cz) and centro-parietal (CP3) regions. In addition, we included interhemispheric motor connectivity (C3–C4), a midline fronto-central connection (Cz–Fz), and bilateral frontal connectivity (F3–F4) to capture broader network effects. This leads to a total of 48 features to represent the PLV. Specifically, the following electrode pairs were utilized:

$$\begin{aligned}\text{Pairs} = \{ &(\text{C3}, \text{F3}),\ (\text{C3}, \text{FC3}),\ (\text{C3}, \text{P3}),\\ &(\text{C3}, \text{Cz}),\ (\text{C3}, \text{CP3}),\ (\text{C3}, \text{C4}),\end{aligned}$$

Table 1
Regions of interest (ROIs) and their corresponding electrode names used for calculating power spectral density, fitting oscillations and 1/*f*, and sample entropy.

Region of Interest (ROI)	Electrode names
Left motor	C3, FC3, CP3
Right motor	C4, FC4, CP4
Central motor	Cz, C3, C4
Left frontal	F3, FC3
Right frontal	F4, FC4
Central frontal	Fz, FCz
Left parietal	P3, CP3
Right parietal	P4, CP4
Central parietal	Pz
Left frontocentral	F3, FC3, C3
Right frontocentral	F4, FC4, C4
Interhemispheric motor	C3, C4, FC3, FC4

$$(\mathrm{Cz}, \mathrm{Fz}),\ (\mathrm{F3}, \mathrm{F4})\ \} \tag{2}$$

The ***Power Spectral Density (PSD)*** quantifies how the power of a signal is distributed across different frequency components, offering insight into neural oscillatory activity. In this study, PSD is estimated using Welch's method, which improves variance reduction by averaging over multiple segments, leading to smoother PSD estimates (Welch, 2003).

The discretely sampled signal x is divided into M segments of length N (here, N = 1000 or 1 Hz resolution given the sampling frequency), with a 50% overlap. A Hamming window function w is applied to each segment to reduce spectral leakage. The Discrete Fourier Transform (DFT) is computed for each segment using the Fast Fourier Transform (FFT) algorithm. The periodogram for each segment is then calculated from the squared magnitude of the DFT. For a given segment k for the signal x and sampling frequency f_s, the periodogram at frequency f is computed as:

$$P_k(f) = \frac{1}{f_s \sum_{n=0}^{N-1} w[n]^2} \left| \sum_{n=0}^{N-1} x_k[n]\, w[n] \exp\left(-j\, 2\pi \frac{f}{f_s} n\right) \right|^2 \tag{3}$$

With w the Hamming window function and in front a normalization factor to compensate for the energy loss caused by applying the window function. Eventually, the average periodograms over all segments are taken:

$$P_{Welch}(f) = \frac{1}{M} \sum_{k=1}^{M} P_k(f) \tag{4}$$

Table 1 lists the Regions of Interest (ROIs) along with the corresponding electrodes used to compute the PSD (average PSD over the electrodes in the ROI). The same frequency bands used for PLV are utilized. The ROIs were selected to cover cortical areas most relevant to motor cortex stimulation, including the left, right, and central motor, frontal, and parietal regions. Left and right frontocentral regions, as well as interhemispheric motor connections, were also included to capture broader motor-network activity and potential bilateral interactions. Note that these ROIs will also be used to compute the entropy features and aperiodic exponent. This leads to a total of 72 features to represent the PSD.

Additionally, the ***aperiodic exponent (slope) of the PSD*** was computed as a feature. The power spectrum, estimated from 1–100 Hz for each region of interest (ROI), was decomposed into periodic (oscillatory) and aperiodic (1/f) components using the Fitting Oscillations & One-Over-F (FOOOF) method (Donoghue et al., 2020). The aperiodic exponent characterizes the rate at which power decreases with increasing frequency. A flatter power spectrum (lower exponent) is associated with higher intrinsic excitability, while a steeper power spectrum (higher exponent) reflects lower excitability (Donoghue et al., 2020). Again, this leads to a total of 12 features.

Sample Entropy is an information-theoretic measure used to quantify the degree of irregularity or unpredictability in a time segment. Lower entropy values are associated with increased excitation/inhibition (E/I) balance, reflecting more regular or ordered signals, whereas higher entropy values indicate reduced E/I balance, corresponding to more complex or irregular signals (Pellegrino et al., 2024).

Mathematically, sample entropy is defined as the negative logarithm of the conditional probability that two subseries of m consecutive data points that are similar (within a tolerance or similarity threshold r) remain similar for subseries of length $(m+1)$. This is expressed as:

$$\mathrm{SampEn}(m, r, N) = -\ln\left(\frac{C_{m+1}(r)}{C_m(r)}\right) \tag{5}$$

where N is the length of the time series ($N = \{x_1, x_2, x_3, \ldots, x_N\}$), and $C_m(r)$ represents the fraction of similar sequences of length m within tolerance r (here excluding the self-matches):

$$C_m(r) = \frac{\left|\{\,(i,j) \mid d\left(X_m(i), X_m(j)\right) \le r,\ i \ne j\,\}\right|}{(N-m)(N-m+1)} \tag{6}$$

$$X_m(i) = \{x_i, x_{i+1}, x_{i+2}, \ldots, x_{i+m-1}\}, \quad 1 \le i \le N-m+1. \tag{7}$$

Here, $d\left(X_m(i), X_m(j)\right)$ is a distance metric between the $X_m(i)$ and $X_m(j)$. The Chebyshev distance (maximum absolute difference) was used as the distance metric, with $r = 0.2$ and $m = 2$.

This leads to a total of 12 features to represent the Sample Entropy, by computing the average entropy of the electrodes in each ROI.

The rsEEG recording, approximately 10 min in duration, is divided into 10 non-overlapping segments, each 1 min long. The features described above were computed for each of these segments. This resulted in 10 samples consisting of 144 features for each patient under each stimulation condition.

Additionally, the study explored adding post-stimulation information into the model. The 10-minute post-stimulation recording is again divided into 10 non-overlapping segments, and the same features were extracted from each segment. Finally, the difference between post- and pre-stimulation feature values, referred to as the delta (Post-Pre) features, was computed to quantify changes induced by the stimulation.

2.5. Baseline model

To establish a performance benchmark, we implemented a random guessing strategy for predicting TEP changes following iTBS and cTBS. This baseline enables a meaningful comparison against our ML models.

For each TEP component and stimulation type, the target variable $y = \Delta\mathrm{TEP}$ is defined as the amplitude change between post-stimulation and pre-stimulation TEP component amplitude:

$$y = \Delta\mathrm{TEP} = \mathrm{TEP}_{\mathrm{post}} - \mathrm{TEP}_{\mathrm{pre}}, \quad \text{for TEP} \in \{\mathrm{N15}, \mathrm{P30}, \mathrm{N45}, \mathrm{P60}, \mathrm{N100}, \mathrm{P180}\} \tag{8}$$

All models were evaluated using 10-fold GroupKFold cross-validation, grouping samples by patient in either train or test to prevent data leakage. For the baseline, we assumed no prior knowledge of the TEP change distribution. Therefore, in each fold, we uniformly sampled prediction values from the observed range of TEP changes in the training set:

$$\hat{y} = \hat{\Delta\mathrm{TEP}} \sim \mathcal{U}\left(\min(\Delta\mathrm{TEP}_{\mathrm{train}}), \max(\Delta\mathrm{TEP}_{\mathrm{train}})\right) \tag{9}$$

To estimate the expected error under random guessing, we performed $M = 1000$ iterations, computing the Mean Absolute Error (MAE)

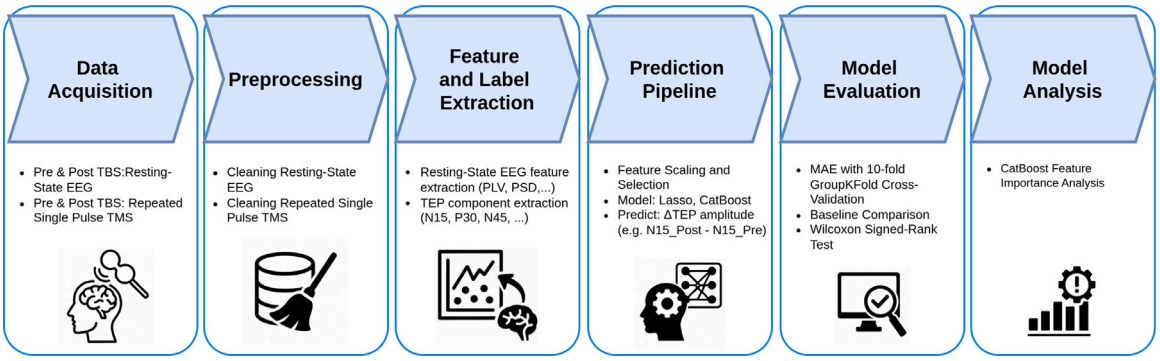

Fig. 2. Overview of the machine learning pipeline. The workflow begins with data acquisition involving resting-state EEG and repeated single-pulse TMS both before and after TBS. Preprocessing steps include artifact cleaning for both EEG and TMS-EEG data. From these data, spectral (e.g., PSD, PLV) and evoked (TEP) features are extracted. These features are then used in a machine learning pipeline to predict changes in TEP component amplitudes (e.g., $N15_{post}$ - $N15_{pre}$). Both linear (Lasso) and nonlinear (CatBoost) models are evaluated using 10-fold GroupKFold cross-validation. The machine learning model performance is compared against the guessing baseline through Wilcoxon signed-rank tests. Finally, feature importance analysis is performed to identify key predictors driving TEP responses to TBS.

between the randomly generated predictions $\Delta\hat{\text{TEP}}$ and the true ΔTEP changes of all S samples in the test fold. The MAE for round n (fold) is computed as:

$$\text{MAE}_n = \frac{1}{M}\sum_{m=1}^{M}\left(\frac{1}{S}\sum_{s=1}^{S}\left|\Delta\text{TEP}_s - \Delta\hat{\text{TEP}}_{s,m}\right|\right) \tag{10}$$

Mean and standard deviation of the MAEs across all folds were used to quantify baseline performance.

2.6. Machine learning modeling

The study designed an ML pipeline to investigate both linear and nonlinear models for predicting changes in TEP components (N15, P30, N45, P60, N100, P180) following iTBS and cTBS. We compared both linear and nonlinear predictive ML models to determine whether TEP changes can be effectively captured through simple feature associations or require the modeling of more complex, nonlinear interactions. An overview of the general ML pipeline is shown in Fig. 2.

2.6.1. Lasso regression

Lasso (Least Absolute Shrinkage and Selection Operator) was selected as the linear model due to its suitability for high-dimensional and low-sample-size settings. Unlike ordinary least squares (OLS) regression, Lasso applies L_1-regularization, which not only mitigates overfitting, but also performs embedded feature selection by shrinking less informative coefficients to zero (Tibshirani, 1996; Hastie et al., 2015). This is particularly beneficial in our case, where some features may be redundant or irrelevant. In contrast, Ridge regression (which uses L_2-regularization) does not enforce sparsity, making interpretation less straightforward. Lasso estimates the regression coefficients $\boldsymbol{\beta}$ by minimizing the following loss function:

$$\hat{\boldsymbol{\beta}} = \arg\min_{\boldsymbol{\beta}}\left[\frac{1}{2m}\sum_{i=1}^{m}\left(y_i - \mathbf{x}_i^{\top}\boldsymbol{\beta}\right)^2 + \alpha\sum_{j=1}^{p}|\beta_j|\right] \tag{11}$$

where m is the number of training samples, p the number of features, $\mathbf{x}_i$ the feature vector for sample i, y_i the corresponding TEP change and α the hyperparameter controlling the strength of L_1-regularization. The L_1 penalty $\sum_j |\beta_j|$ encourages sparsity in the coefficient vector, driving many coefficients to zero, effectively performing feature selection.

Following the baseline, we employed a 10-fold GroupKFold cross-validation strategy (grouping by patient). In each round, correlation-based feature pruning was performed on the training set X_{train} by computing the correlation matrix and removing one feature from any highly correlated features ($|r| > 0.9$), to reduce redundancy. After pruning, the number of retained features (mean ± SD across rounds) was 83.8 ± 5.5 (cTBS) and 86.9 ± 3.2 (iTBS) for pre-stimulation rsEEG, and 62.1 ± 4.9 (cTBS) and 53.8 ± 1.5 (iTBS) for delta (post–pre) features.

An inner 5-fold cross-validation grid search was used to tune the optimal value of α. Lasso was then trained on the pruned and normalized training data using the selected α, and predictions were made on the test set. Performance was evaluated using MAE, and results were aggregated across folds to report the mean and standard deviation.

2.6.2. CatBoost regression and feature importance

The second pipeline employed a combined Recursive Feature Elimination (RFE) for feature selection with CatBoost for nonlinear regression. In each cross-validation fold, RFE was first used to select an optimal subset of features. This was achieved by iteratively training a Lasso model and removing the least important features based on their coefficient magnitudes. The resulting feature subset was then used to train the final CatBoost regression model.

CatBoost is a gradient-boosting algorithm that builds an ensemble of decision trees. It uses an iterative procedure to fit new trees that predict the residuals (errors) of the current model. In each iteration t, the model is updated as:

$$F_{t+1}(\mathbf{x}) = F_t(\mathbf{x}) + \eta \cdot h_t(\mathbf{x}) \tag{12}$$

where $F_t(\mathbf{x})$ is the current model, η the learning rate, and h_t a new weak learner (oblivious tree) trained to fit the negative gradient (residuals) of the current model.

CatBoost was chosen over other tree-based ensemble methods, such as XGBoost, due to its ordered boosting with permutation-based processing, which helps to reduce overfitting, especially in small datasets (Prokhorenkova et al., 2018). In ordered boosting, residuals for a given sample are calculated using a model trained only on preceding samples in a random permutation. This prevents target leakage and improves the model's ability to generalize.

The model was similarly evaluated using 10-fold GroupKFold cross-validation. CatBoost was run with its default hyperparameters, including a maximum of 1000 iterations, a maximum tree depth of 6, and an L2 leaf regularization of 3. The learning rate was left to CatBoost's automatic selection, which adapts to the dataset and number of iterations.

To understand which features drove the model's predictions, we analyzed feature importances using CatBoost's PredictionValuesChange method. This method quantifies a feature's impact by measuring the total change in prediction values across all tree splits involving that feature. A higher feature-importance score indicates that changes in this feature's value have a larger average impact on the model's predictions.

Table 2
TEP component amplitudes (mean ± standard deviation) for cTBS and iTBS, before (Pre) and after (Post) stimulation.

Component	cTBS		iTBS	
	Pre	Post	Pre	Post
N15	−0.600 ± 0.053	−1.090 ± 0.052	−0.590 ± 0.036	−0.520 ± 0.070
P30	0.640 ± 0.020	0.680 ± 0.016	0.720 ± 0.042	0.760 ± 0.089
N45	−1.390 ± 0.020	−1.730 ± 0.015	−1.640 ± 0.042	−1.730 ± 0.089
P60	0.670 ± 0.024	0.860 ± 0.015	0.680 ± 0.045	0.210 ± 0.097
N100	−0.990 ± 0.038	−0.890 ± 0.087	−1.410 ± 0.043	−0.920 ± 0.007
P180	1.390 ± 0.039	1.270 ± 0.032	1.350 ± 0.014	1.350 ± 0.097

Table 3
Mean absolute error (mean ± standard deviation) across patients for Lasso regression models predicting TEP component changes after cTBS and iTBS using 10-fold GroupKFold cross-validation. Models were trained on either pre-stimulation rsEEG features ("Pre Only") or delta features ("Post-Pre").

Component	cTBS			iTBS		
	Pre Only	Post-Pre	Baseline	Pre Only	Post-Pre	Baseline
N15	0.94 ± 0.66**	0.88 ± 0.65**	1.28 ± 0.60	0.95 ± 0.42	0.78 ± 0.28**	0.96 ± 0.22
P30	0.62 ± 0.38**	0.55 ± 0.37**	0.99 ± 0.18	1.04 ± 0.62	0.86 ± 0.30*	1.03 ± 0.26
N45	0.42 ± 0.22	0.40 ± 0.21	0.51 ± 0.13	0.69 ± 0.43**	0.95 ± 0.51	0.98 ± 0.26
P60	0.53 ± 0.27**	0.62 ± 0.54**	1.04 ± 0.33	0.62 ± 0.26	0.65 ± 0.21	0.64 ± 0.13
N100	0.68 ± 0.47**	0.71 ± 0.46**	1.21 ± 0.27	0.48 ± 0.25**	0.75 ± 0.41	0.88 ± 0.20
P180	1.04 ± 0.51	0.92 ± 0.59**	1.26 ± 0.44	0.74 ± 0.46**	0.75 ± 0.54**	1.31 ± 0.27

Statistically significant improvements over the baseline (Wilcoxon signed-rank test) are indicated:
* $p < 0.05$.
** $p < 0.01$.

For a single split on a feature F, the importance contribution is calculated based on the reduction in prediction variance. Let c_1, c_2 denote the total sample weights in the left and right child nodes, respectively, and let v_1, v_2 be the prediction values assigned to these nodes. The average prediction at the split is:

$$avr = \frac{v_1 c_1 + v_2 c_2}{c_1 + c_2} \tag{13}$$

The importance gain (ΔI_F) from this split is the weighted variance of the child node predictions relative to the parent's average prediction:

$$\Delta I_F = (v_1 - avr)^2 \cdot c_1 \; + \; (v_2 - avr)^2 \cdot c_2 \tag{14}$$

The total raw importance of feature F is the sum of these gains over all splits on F across all trees in the ensemble:

$$I_F^{\text{raw}} = \sum_{\text{splits}} \Delta I_F \tag{15}$$

Finally, these raw importance scores are normalized so that the sum of all feature importances equals 100. To combine importances across all folds, we took the mean normalized importance and ranked the features.

3. Results

3.1. TEP responses to cTBS and iTBS

The average TEP responses and their standard deviations across patients are illustrated in Figs. 3 and 4 for cTBS and iTBS, respectively. These plots depict the temporal dynamics of the waveforms, highlighting the amplitudes of the different TEP components (N15, P30, N45, P60, N100, and P180) and the differences between pre- and post-stimulation responses to single pulse TMS. The TEP responses are averaged over all 150 single pulses for each patient, and the group-level average and standard deviation are computed across patients. The analysis used the average of the C3, C1, and Cz channels, selected due to their proximity to the stimulation site (cortex), which was the region of interest in this study.

Statistical analysis of TEP component changes is available in the study by Carrette et al. (2025). As a summary, the mean amplitudes and standard deviations for each component across patients, both pre- and post-stimulation, are provided in Table 2, offering a quantitative overview of the changes induced by cTBS and iTBS.

To further characterize the relationship between pre- and post-stimulation TEP amplitudes, we computed the concordance correlation coefficient (CCC). Results are provided in Supplementary Figure S1. As CCC is typically used for test–retest reliability, the metric is not ideally suited as a reliability metric in a pre–post intervention design. Therefore, the values here should be interpreted cautiously as descriptive indicators of concordance rather than strict reliability, given the presence of potential stimulation-induced effects.

3.2. Predicting TEP component changes

We evaluated the ability of Lasso and CatBoost regressors to predict TBS-induced changes in TEP components, benchmarking their performance against the baseline model. Predictions were based on two types of feature sets: (1) pre-stimulation rsEEG features ("Pre Only") and (2) delta rsEEG features ("Post-Pre"). Performance was assessed separately for the cTBS and iTBS protocols using mean absolute error (MAE) with standard deviations from 10-fold GroupKFold cross-validation as listed in Tables 3 and 5.

To statistically evaluate the added value of the ML models, we used Wilcoxon signed-rank tests comparing fold-wise MAE distributions of each model against the baseline. This non-parametric test allows us to determine whether the observed improvements are statistically significant ($p<0.05$), accounting for within-subject dependencies across folds. Significance levels are indicated as follows in Tables 3 and 5: * $p<0.05$ and ** $p<0.01$.

3.2.1. Lasso regression results

The Lasso regression model exhibited variable predictive performance across TEP components, but outperformed the baseline in almost all components, as summarized in Table 3. Components with higher baseline MAE values tended to exhibit greater absolute errors in model predictions, reflecting the greater variability of change for that particular component.

Under the cTBS protocol, statistically significant improvements over the baseline were observed for N15, P30, P60 and N100. For N45 and

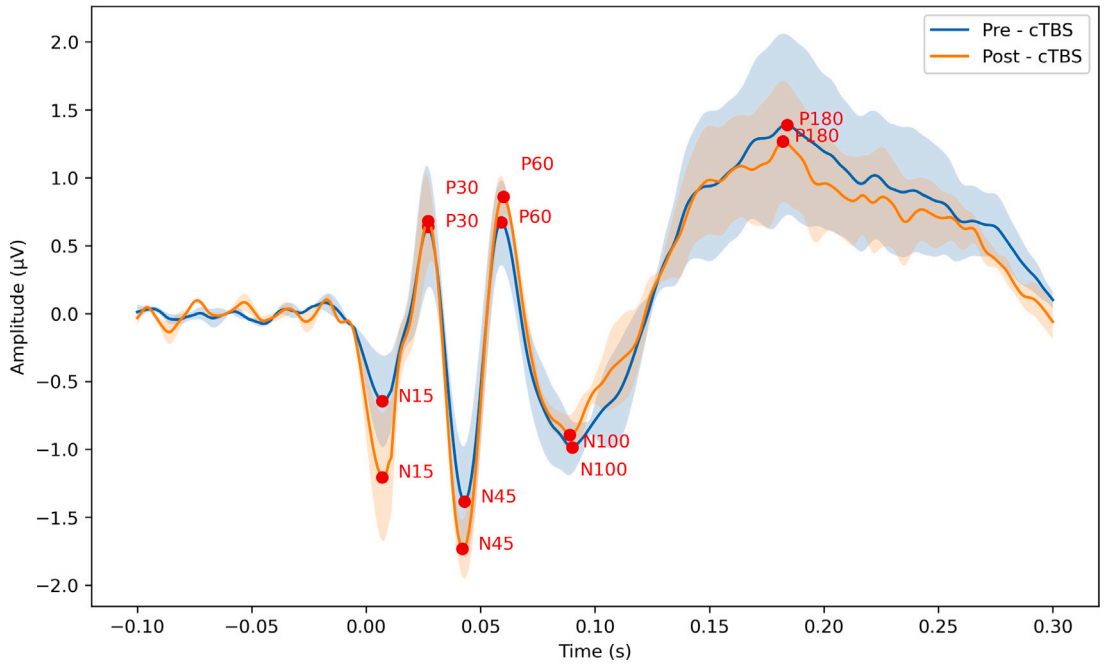

Fig. 3. Average TMS-evoked potentials (TEPs) across patients before (pre) and after (post) continuous theta burst stimulation (cTBS). Solid lines represent the grand-average waveforms, and shaded areas indicate ±1 standard deviation across participants. The peaks of the TEP components of interest (N15, P30, N45, P60, N100, and P180) are marked on the waveforms.

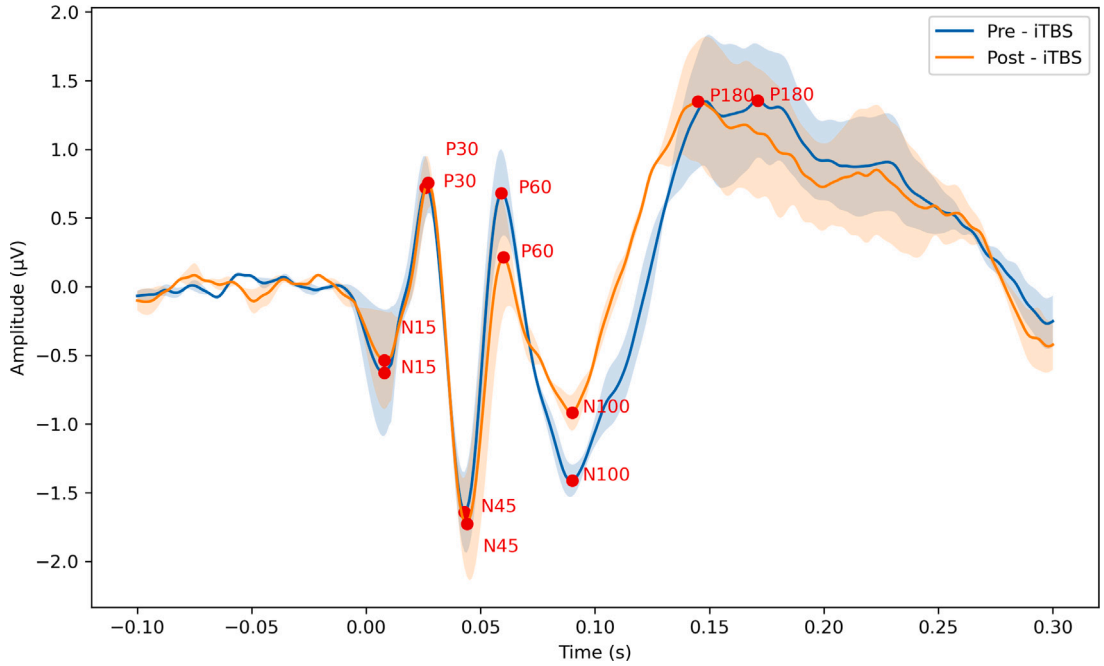

Fig. 4. Average TMS-evoked potentials (TEPs) responses across patients before (pre) and after (post) intermittent theta burst stimulation (iTBS). Solid lines represent the grand-average waveforms, and shaded areas indicate ±1 standard deviation across participants. The peaks of the TEP components of interest (N15, P30, N45, P60, N100, and P180) are marked on the waveforms.

P180, the model demonstrated a performance gain over the baseline, although it was not statistically significant.

Using delta features as input improved the performance for predicting certain components. The Lasso model now statistically significantly outperformed the baseline for P180, in addition to maintaining significance for N15, P30, P60, and N100. However, improvements relative to the "Pre Only" model were not statistically significant (when comparing the 2 models on different feature inputs). The N45 remained the only component for which neither feature set achieved statistically significant improvement over the baseline, although the delta model seems to approach significance ($p = 0.052$).

Under the iTBS condition, the Lasso model using pre-stimulation features yielded significant improvements for N45, N100 and P180. In contrast, model performance for N15, P30, and P60 did not significantly differ from the baseline, suggesting limited predictive value in pre-stimulation features for these components under iTBS.

The use of delta features did not uniformly increase the predictive performance of the model. Delta features improved predictions for

Table 4
Permutation test results for Lasso regression models. Reported values are permutation p-values assessing whether model performance exceeded chance levels. Significant results are shown in bold ($p < 0.05$).

Component	cTBS	iTBS
N15	0.956	0.652
P30	0.466	0.872
N45	0.286	0.202
P60	**0.023**	0.499
N100	0.408	**0.012**
P180	0.897	**0.002**

N15 and P30, but were not statistically significant over using the "Pre Only" model. However, the other four components showed negligible or slightly worse performance with delta features. Compared to the baseline, the delta model showed significant performance improvement in N15, P30 and P180. For P60, neither feature set outperformed the baseline significantly.

3.2.2. Permutation-based validation

To further assess model performance and overfitting, permutation testing was conducted for the Lasso regression models. Target labels were randomly permuted 1000 times, and the full nested cross-validation pipeline was repeated to generate null distributions of model performance.

The results further confirm the component- and protocol-specific predictive performance. Under the iTBS protocol, performance significantly exceeded chance levels for ΔN100 (p = 0.012) and ΔP180 (p = 0.002). Under cTBS, significant performance was observed for ΔP60 (p = 0.023). Predictions for the remaining components did not significantly outperform permutation baselines.

These findings indicate that predictive information contained in resting-state EEG is selectively expressed in specific neurophysiological markers rather than uniformly across all TEP components. A summary of permutation results is provided in Table 4, while full null distributions are provided in Supplementary Figures S2 and S3.

3.2.3. CatBoost regression results

The CatBoost regression model outperformed the baseline across most TEP components, as shown in Table 5. As observed previously with Lasso, the model's mean MAE tended to be higher for components with higher baseline MAE values, indicating greater variability in TEP responses.

Under the cTBS condition, the CatBoost model trained on pre-stimulation features achieved statistically significant improvements over the baseline for five out of six components: N15, P30, P60, N100 and P180. Only for predicting N45, the model did not significantly outperform the baseline. Using delta features, the CatBoost model significantly outperformed the baseline for all six cTBS components, including N45, which was not the case with the Lasso model. Furthermore, the delta features model yielded significantly better performance than the pre-stimulation features model for the N45 component, but not for the other components.

Under the iTBS condition, the "Pre Only" CatBoost model showed a significant improvement only for N100. No other components showed statistically significant improvements with pre-stimulation features alone.

Using delta features, the CatBoost significantly improved performance for N15, N45 and P180. However, these improvements were not observed consistently across all components.

When directly comparing the performance of CatBoost with Lasso, no significant performance gains were observed for either the "Pre Only" or "Post-Pre" feature sets across all components. The closest was N45 under cTBS using delta features with p = 0.097.

3.3. Feature importance analysis for cTBS

To identify the most influential features in predicting TEP changes following cTBS, a feature importance analysis was conducted on the CatBoost regression model. For cTBS, the importance scores of individual features, along with the predicted versus actual TEP changes in the test folds, are illustrated in Fig. 5.

Across multiple TEP components, PLV in the Theta and High Gamma frequency bands between the central (C3, stimulation site) and frontal/parietal electrodes consistently emerged as the most significant predictors. In addition, PSD in the Low Beta and Low Gamma bands, particularly in mid-parietal and frontal regions, were recurrently identified as key predictive features.

For N15, important features included interhemispheric connectivity, such as PLV in the Theta band between F3–F4, C3–C4, C3–CP3, and Cz–Fz, as well as PLV in the High Gamma band between Cz–Fz and C3–F3. Additionally, PSD in the Low Gamma band within the right frontal region and Low Beta in the mid-parietal region demonstrated notable importance. For P30, PSD in the Low Gamma band in mid-frontal and right frontal regions showed particularly high importance, along with PLV in the Low Beta band between C3–FC3. For N45, FOOOF of the left motor region was the highest predictor, followed by PLV in High Beta between C3–Cz and PSD in Low Gamma in the mid-frontal region. Regarding P60, PSD in the High Beta band in the right frontal region and Low Gamma band in the mid-frontal region were the two most dominant features. For N100, PSD in the Low Gamma band in the mid-frontal region and PLV in the Theta band between C3–FC3 emerged as top predictors. Finally, for P180 the most dominant predictor was PSD in the Alpha band in the right motor region.

To further assess the robustness of these findings, SHAP analyses were performed. The SHAP-based feature importance results showed largely consistent patterns with the CatBoost feature-importance analysis. However, it is important to note that SHAP values reflect feature contributions to model predictions rather than causal relationships, and should therefore be interpreted with caution, particularly given the limited sample size. Full SHAP results are provided in Supplementary Figure S4.

3.4. Feature importance analysis for iTBS

Similarly, the importance scores of individual features, along with the predicted versus actual TEP changes of the test folds, for iTBS are illustrated in Fig. 6.

The most influential predictors across different TEP components were PLV and PSD features in the Beta, Gamma, and Theta frequency bands, particularly in motor and frontal regions.

For N15, the strongest predictor was PSD in the Theta band within interhemispheric motor regions, followed by PLV in the High Beta band between C3-C4 and PLV in the High Gamma band between C3-FC3. For P30, PLV in the high beta band between C3-CP3 emerged as the top feature, along with PLV in the theta band between C3-F3 and C3-FC3. These findings highlight the relevance of theta connectivity in motor-prefrontal networks. For N45, PLV in the High Gamma band between F3-F4 showed the highest importance. For P60, PLV in the alpha band between C3-F3 was the most dominant feature. For N100, PSD in the High Beta band within the right motor cortex and PLV in the High Gamma band between F3-F4 were identified as key predictors. Finally, for P180, PSD in the alpha band within the right motor region was the most dominant feature by far compared to the others.

Similarly, SHAP analyses for the iTBS condition showed broadly consistent trends observed in the CatBoost feature-importance analysis. The full SHAP results are provided in Supplementary Figure S5.

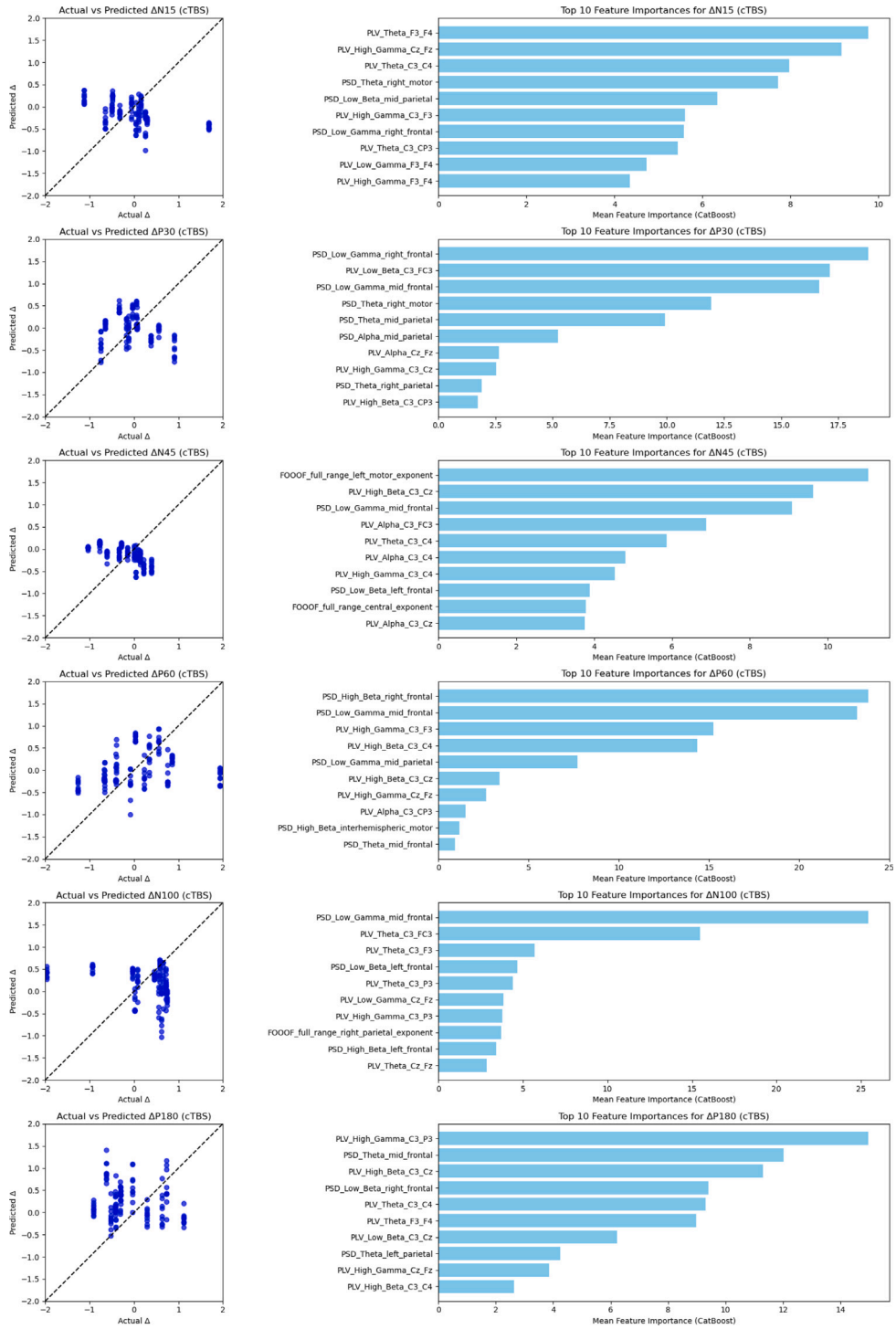

Fig. 5. Predictive Performance and Feature Importance Analysis for TEP Components under cTBS Protocol. Left column: Scatter plots showing predicted versus actual *Δ*TEP amplitudes across cross-validation folds, illustrating model performance for each TEP component. The dashed line indicates the identity line. **Right column:** Bar charts showing the top 10 pre-stimulation resting-state EEG features for each TEP component, ranked by mean feature importance across cross-validation folds (CatBoost). Features are ordered from highest to lowest importance.

4. Discussion

The results of our study demonstrate that when linear (Lasso) and nonlinear (CatBoost) ML models are used to predict TEP component changes following iTBS and cTBS, consistently lower mean absolute errors are found than a naive guessing approach. This suggests that the rsEEG features contain predictive information that can be leveraged to forecast individual TEP responses to TBS.

Predictive performance was consistently more robust for cTBS-induced changes than for iTBS. Across feature sets and models, both approaches achieved statistically significant improvements over the baseline for a greater number of components under cTBS, particularly N15, P30, P60, and N100. This difference may reflect more consistent neurophysiological effects of cTBS across individuals or greater alignment between current rsEEG features and the physiological processes influenced by cTBS

Table 5
Mean absolute error (mean ± standard deviation) across all patients for CatBoost regression models predicting TEP component changes after cTBS and iTBS, evaluated using 10-fold GroupKFold cross-validation. Models were trained on either pre-stimulation rsEEG features ("Pre Only") or delta rsEEG features ("Post-Pre").

Component	cTBS			iTBS		
	Pre Only	Post-Pre	Baseline	Pre Only	Post-Pre	Baseline
N15	0.76 ± 0.70**	0.81 ± 0.84**	1.28 ± 0.60	0.88 ± 0.43	0.78 ± 0.19**	0.96 ± 0.22
P30	0.54 ± 0.37**	0.59 ± 0.34**	0.99 ± 0.18	1.00 ± 0.46	0.93 ± 0.31	1.03 ± 0.26
N45	0.50 ± 0.26	0.34 ± 0.15**	0.51 ± 0.13	0.84 ± 0.49	0.64 ± 0.34*	0.98 ± 0.26
P60	0.57 ± 0.25**	0.64 ± 0.51**	1.04 ± 0.33	0.79 ± 0.30	0.67 ± 0.24	0.64 ± 0.13
N100	0.60 ± 0.51**	0.59 ± 0.52**	1.21 ± 0.27	0.62 ± 0.44	0.90 ± 0.40	0.88 ± 0.20
P180	0.88 ± 0.57**	0.91 ± 0.62*	1.26 ± 0.44	0.76 ± 0.32**	1.01 ± 0.55*	1.31 ± 0.27

Statistically significant improvements over the baseline (Wilcoxon signed-rank test) are indicated:
* $p < 0.05$.
** $p < 0.01$.

Some components, mostly components modulated by iTBS, proved more challenging to predict, as no statistically significant improvement was found over the baseline. Further, no significant improvement over the baseline was found for P60 under iTBS, regardless of the model or feature set used. Permutation testing further confirmed the component-protocol-specific effects, demonstrating that predictive signal in resting-state EEG is selectively expressed rather than uniformly distributed across neurophysiological outcomes. This selective predictability suggests that baseline brain-state dynamics more strongly influence certain TEP markers, whereas others may depend on factors not captured by resting-state measures, such as stimulation-specific mechanisms, high inter-individual variability, or weak coupling to intrinsic network features.

Under Lasso regression, the benefit of using delta features over pre-only features was inconsistent, with some components showing modest performance gains and others exhibiting degradation. Specific components, such as P180 under cTBS and N15 and P30 under iTBS, exhibited significant gains over the baseline using delta features, which was not the case in the pre-only model. This suggests that post-stimulation information may add value for certain components, though this benefit appears to be highly component- and protocol-specific. Because delta features incorporate post-stimulation information, they are not directly suitable for prospective prediction but may provide insight into stimulation-induced network changes and may serve as mechanistic probes, particularly when larger datasets become available.

CatBoost demonstrated more consistent performance gains with delta features, particularly under cTBS. In this setting, the delta-based CatBoost model significantly outperformed the baseline for all six TEP components, including N45, where Lasso did not achieve significance. This highlights the potential of more advanced models like CatBoost in capturing nonlinear interactions between EEG features and TEP changes.

When directly comparing CatBoost to Lasso, no systematic or statistically significant performance advantage was observed, suggesting that both linear and nonlinear approaches are viable. For certain conditions (e.g., N45 under cTBS using delta features), CatBoost approached significance, suggesting that nonlinear models may offer advantages for components that may be influenced by higher-order interactions.

The absence of consistent performance improvements when incorporating delta features may reflect the dynamic and heterogeneous nature of post-TBS cortical states. Immediately after stimulation, rsEEG may capture transient network responses that vary across individuals and evolve over time as plasticity-related processes unfold. Such variability can introduce additional noise into delta-based predictors, particularly when recordings are obtained within a relatively short post-stimulation window. Moreover, TBS-induced plasticity is known to show substantial inter-individual variability and even opposite responses across participants, which may further reduce the stability of stimulation-induced feature changes. Consequently, while delta features may provide insight into stimulation-induced network modulation, they may not reliably enhance predictive performance in small datasets. Future studies with larger cohorts and more systematic characterization of post-stimulation dynamics may help clarify whether changes in resting-state activity can serve as stable markers of TBS-induced cortical modulation.

The feature importance analyses provided further insights into which aspects of rsEEG best predict TEP changes. Across both cTBS and iTBS, PLV features in the Theta and Gamma frequency bands between motor and frontal/parietal regions consistently ranked highly, underscoring the importance of functional connectivity in these oscillatory ranges. This pattern may reflect TBS-induced modulation of networks involved in motor and cognitive processing. PSD features in the Beta and Gamma bands also frequently emerged as important predictors, particularly in frontal and parietal regions, suggesting a role of oscillatory power related to sensorimotor integration and executive function. Interestingly, sample entropy did not emerge as an important predictor for any component, which may indicate that more global measures of signal irregularity are less directly related to TBS-induced modulation than frequency-specific connectivity and power features. In addition, entropy estimates are sensitive to preprocessing choices (e.g., filtering and artifact removal), which can alter signal complexity, while regional averaging within ROIs may reduce variability and further limit their discriminative value.

Importantly, it should be noted that feature importance measures derived from machine-learning models reflect the contribution of predictors to model performance and their statistical association with the predicted outcome, rather than direct neurophysiological causation. Consequently, the identified rsEEG features should be considered candidate markers associated with variability in TBS-induced cortical responses rather than mechanistic drivers of neuromodulatory effects. These findings are therefore hypothesis-generating and may guide future studies aimed at testing causal relationships using targeted experimental manipulations or intervention-based designs.

The predictive framework focused exclusively on active stimulation conditions (iTBS and cTBS) and did not include the sham condition in the modeling pipeline. This choice was motivated by the objective of predicting neuromodulatory effects induced by TBS, as sham stimulation is not expected to produce systematic plasticity-related changes in TEP responses. Consistent with this, the original dataset did not observe systematic TEP modulation following the control condition. Nevertheless, spontaneous fluctuations in TEP amplitudes cannot be entirely excluded, and future work could use sham-derived ΔTEP distributions as a reference for background variability.

Although the present study focused on predicting post-stimulation TEP amplitude changes using rsEEG features, additional pre-TBS TEP characteristics (including latency shifts, scalp topography, and time–frequency dynamics) may contain complementary predictive information. However, to maintain a clear focus on rsEEG information and to limit model dimensionality, models were restricted to rsEEG predictors. Future work may extend this predictive framework by incorporating such features when larger datasets become available.

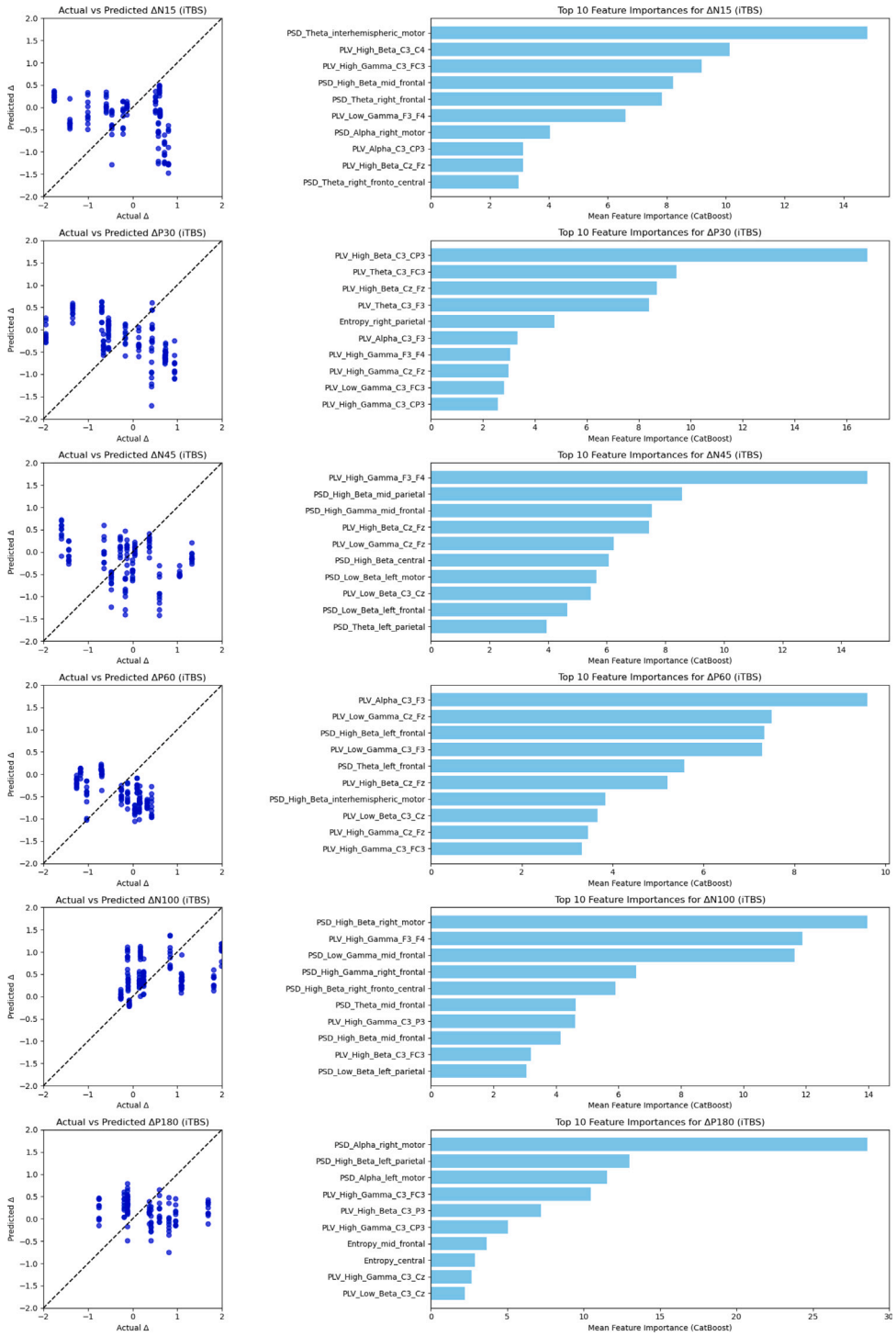

Fig. 6. Predictive Performance and Feature Importance Analysis for TEP Components under iTBS Protocol. Left column: Scatter plots showing predicted versus actual ΔTEP amplitudes across cross-validation folds, illustrating model performance for each TEP component. The dashed line indicates the identity line. **Right column:** Bar charts showing the top 10 pre-stimulation resting-state EEG features for each TEP component, ranked by mean feature importance across cross-validation folds (CatBoost). Features are ordered from highest to lowest importance.

TMS and TBS parameters play a critical role in the interpretation of TMS–EEG responses. At the time of data acquisition, a fixed subthreshold stimulation intensity (80% rMT) was applied across participants and sessions. However, the resulting level of cortical engagement may vary between individuals. Stimulation dosing can strongly influence perturbation strength, signal quality, and the reproducibility of TEPs. Higher intensities increase the magnitude, spatial propagation, and reliability of cortical responses (Kerwin et al., 2018; Casarotto et al., 2010; Lioumis et al., 2009), and recent work demonstrates dose-dependent increases in early local TEP amplitudes together with improved test–retest reliability metrics such as concordance correlation coefficients (CCC) (Chen et al., 2025). TMS–EEG-guided thresholding approaches indicate that effective cortical activation emerges at specific stimulation intensities, reflecting recruitment of cortical networks (Casarotto et al., 2022). By identifying the minimum intensity required to elicit reliable cortical responses (e.g., peak-to-peak TEP thresholds), these

approaches provide an alternative to motor threshold–based dosing and support individualized stimulation parameters tailored to cortical responsiveness rather than corticospinal excitability (Casarotto et al., 2022; Lioumis and Rosanova, 2022; Rissanen et al., 2026). Accordingly, individualized dosing based on early evoked responses may optimize cortical engagement reliability, enhance the sensitivity of TMS–EEG measures and potentially also the predictive power of our models. Therefore, incorporating EEG-guided dosing and targeting strategies represents an important direction for future studies.

While higher intensities enhance response reliability, they also increase muscle activation and sensory co-activation, which can contaminate later components. Thus, stimulation intensity selection represents a trade-off between maximizing cortical perturbation and minimizing artifacts. TEPs are particularly susceptible to contamination from craniofacial muscle activity, auditory responses, and somatosensory reafference, and supra-threshold stimulation may introduce proprioceptive feedback that influences later EEG responses (Fecchio et al., 2017). Therefore, new methodological frameworks emphasize optimizing stimulation parameters to maximize cortical perturbation while minimizing artifacts (Casarotto et al., 2022; Lioumis and Rosanova, 2022). In the present study, subthreshold stimulation was selected to reduce peripheral confounds. Further, our predictive modeling framework focused on relative post–pre changes in TEPs, making the influence of consistent sensory or peripheral confounds likely to be reduced (as stable contributions present in both recordings would be attenuated). Nonetheless, individualized EEG-guided optimization of stimulation intensity and coil orientation may further improve response reliability across participants and sessions and enhance sensitivity to brain-state-dependent TEP prediction.

Standard deviations remained high across test folds, reflecting inter-subject variability in stimulation response and the limited sample size of the dataset. However, the variability in responses also highlights the need for methods, such as those in this study, that can help to predict a patient stimulation outcome in order to make TBS a reliable stimulation technique.

Predicting individual cortical responses prior to stimulation (e.g., whether N45 amplitude will increase following cTBS) represents an important step toward personalized TBS. Such predictions could inform clinical decision-making, for example, by postponing or adjusting stimulation when a beneficial neurophysiological response is unlikely. Emerging evidence supports the functional relevance of specific TEP components. For instance, N100 amplitude has been associated with treatment response in major depressive disorder (Sheen et al., 2024), while higher N45 amplitudes over M1 have been linked to faster stop-signal reaction times (Zhu et al., 2024). While prior studies have linked TEP components to behavioral and clinical outcomes, the present study does not directly assess such relationships. Therefore, these references should be interpreted as contextual background rather than evidence of functional or translational relevance within the current dataset. As research continues to clarify the relationships between TEP amplitudes and behavioral, motor, cognitive, and clinical outcomes, predictive modeling of TEP changes becomes more important. This, in turn, could enhance the development of individualized neuromodulation strategies.

4.1. Limitations

Several limitations should be acknowledged, highlighting areas for future research and underscoring the challenges inherent in studying TMS-EEG responses.

The timing of TMS pulses relative to the phase of ongoing neural oscillations can potentially influence TEP amplitudes (spike time-dependent stimulation). For instance, stimulation at the negative peak of the sensorimotor μ-rhythm has been shown to elicit larger MEP amplitudes than stimulation at the positive peak (Desideri et al., 2019). This variability introduces uncertainty in the interpretation of TEP changes, as the phase of neural oscillations at the time of stimulation is not controlled in this study. To mitigate this, we averaged TEP responses over 150 randomly timed single-pulse TMS trials, which helps reduce phase-dependent variability. However, future studies could investigate phase-locked stimulation protocols to further mitigate this effect.

An additional limitation relates to stimulation dosing. Although a fixed subthreshold intensity (80% rMT) was chosen to minimize peripheral artifacts and sensory contamination, this approach does not guarantee equivalent cortical perturbation across participants. Recent methodological work suggests that EEG-guided optimization of stimulation intensity and coil orientation, based on early evoked responses, may improve perturbation reliability and reproducibility. Variability in perturbation strength may also influence the detectability of brain-state-dependent effects. Future studies incorporating individualized dosing strategies based on real-time EEG guidance and early component thresholding may enhance the robustness and sensitivity of TMS-EEG measures (Casarotto et al., 2022; Lioumis and Rosanova, 2022).

In this study, ROI- and electrode-pair-based features were deliberately selected to focus on regions known to be involved in TMS propagation and TBS-induced modulation. This hypothesis-driven approach reduces dimensionality and mitigates the risk of overfitting, which is particularly important given the limited sample size. However, restricting feature extraction to predefined regions may bias the model toward prior assumptions and limit the discovery of broader or unexpected predictive patterns. Future work with larger datasets could therefore benefit from more exploratory approaches, such as whole-brain connectivity analyses or network-level features derived from connectivity matrices.

The sample size of 15 participants is relatively small given the known inter- and intrasubject variability in TBS responses. However, it is appropriate for an exploratory investigation and is consistent with sample sizes reported in comparable TMS-EEG studies. Conducting a prospective power analysis for the present study is difficult because, to our knowledge, no previous work has attempted to predict TEP component changes following TBS using resting-state EEG features, making reliable effect size estimates unavailable. To mitigate overfitting risks associated with the limited cohort size, the rsEEG recordings were segmented into multiple epochs, and model evaluation was performed using a 10-fold GroupKFold cross-validation strategy that strictly grouped samples by participant to prevent data leakage. In addition, regularized modeling approaches (Lasso and CatBoost) were employed because of their robustness in high-dimensional, low-sample-size settings. However, it is important to emphasize that, despite these precautions, performance estimates remain inherently uncertain and cannot fully mitigate the fundamental statistical limitations of small sample sizes. Therefore, the current findings should be regarded primarily as hypothesis-generating. Validation with larger datasets and independent cohorts will be essential to confirm these results and enhance the generalizability of the predictive models.

An additional limitation concerns the inclusion of only male participants. This decision was made a priori in the broader study from which this dataset originates to minimize variability related to menstrual cycle–associated fluctuations in cortical excitability, which have been shown to influence TMS and TBS responses. While this approach reduced potential inter-session variability in this exploratory cohort, it restricts the generalizability of the findings to mixed-sex populations. Sex-related differences in resting-state EEG characteristics and neuromodulatory responsiveness may influence both predictive features and TEP outcomes. Future studies should therefore plan mixed-sex cohorts to improve generalization.

The preprocessing of TMS-EEG data is a critical step that can significantly influence the resulting TEP components. The lack of a standardized preprocessing pipeline across studies has led to considerable variability in TEP measurements, complicating comparisons and reproducibility. To mitigate this, we adopted the TESA pipeline, which

has been shown to reduce variability and improve reliability compared to alternative methods (Brancaccio et al., 2024). By following state-of-the-art cleaning steps and maintaining consistency in preprocessing across all participants, we aimed to minimize the impact of preprocessing variability on our results. Nevertheless, ICA-based artifact removal is not perfect and may also eliminate EEG components containing physiologically relevant neural activity, a limitation that cannot be fully controlled and may introduce residual bias. The choice of preprocessing steps therefore remains an area of active debate, and future studies should continue to refine and standardize these methods.

Further, sensory co-stimulation is an inherent limitation of TMS-EEG, as it may contribute to later components. In the present study, auditory masking and foam padding were used to attenuate sensory input, and ICA-based artifact removal was applied to reduce muscle and peripheral artifacts. Nevertheless, residual sensory contributions cannot be fully excluded. Because our analyses focused on post–pre changes rather than absolute amplitudes, the influence of consistent sensory or peripheral confounds is likely reduced (as stable contributions present in both recordings would be attenuated). However, future work could incorporate realistic coil click controls or dedicated sensory evoked potential recordings to further quantify sensory contributions.

While feature importance analysis, such as the one performed in this study, is a valuable technique for identifying influential predictors, it has inherent limitations. Feature importance scores provide insights into which features contribute most to the model's predictions, but do not fully elucidate the underlying neurophysiological mechanisms. For example, while PLV in the Theta band may emerge as a highly important feature, the specific nature of its relationship with TEP changes (e.g., whether it reflects excitatory or inhibitory processes) remains unclear. Similarly, the limited contribution of entropy-based features may reflect sample-specific effects rather than a true lack of relevance. Feature-importance rankings may vary with larger and more heterogeneous datasets (mixed-sex cohorts). In small-sample settings, correlations between predictors and inter-individual variability can lead to unstable feature selection and inconsistent ranking across cross-validation folds. While leave-one-participant-out validation yielded largely similar top predictive features, this consistency should be interpreted with caution given the limited sample size. With larger cohorts, more robust and reproducible feature-importance patterns may emerge, and additional predictive features not detectable in the present sample may become evident. Therefore, given the exploratory nature of this work, the feature-importance results should be interpreted primarily as hypothesis-generating.

5. Conclusion

Given the high inter- and intra-subject variability in TBS responses, predicting individual neurophysiological outcomes is crucial for advancing personalized neuromodulation. This study demonstrates the feasibility of using machine learning with pre-stimulation rsEEG features to predict TEP amplitude changes following iTBS and cTBS. Both linear (Lasso) and nonlinear (CatBoost) models consistently outperformed a random baseline, showing that meaningful structure in rsEEG can be leveraged for forecasting. Prediction accuracy, however, varied across TEP components and protocols: cTBS-induced changes were more reliably predicted than those from iTBS, while certain components (e.g., P60 under iTBS) remained particularly difficult to model. Permutation-based validation further demonstrated that predictive signal was component-specific rather than universal, suggesting that only selected neurophysiological markers are robustly linked to current baseline brain-state dynamics. No systematic advantage was found for using delta features (post- vs. pre-stimulation feature difference) over pre-stimulation only features, suggesting that the predictive value of post-stimulation information may be component- and protocol-specific.

Further, by analyzing the CatBoost model, we demonstrated that pre-stimulation rsEEG features, particularly those related to functional connectivity (e.g., Phase Locking Value, PLV) and spectral power (e.g., Power Spectral Density, PSD), can provide insights into individual TEP responses. Feature importance analysis revealed that connectivity measures in the theta, beta, and gamma frequency bands, particularly between motor and frontal regions, were among the most influential predictors of TEP changes. This highlights the importance of inter-regional communication and oscillatory activity in shaping TBS-induced cortical responses. However, feature importance measures derived from machine-learning models should be interpreted in context as they reflect the contribution of predictors to model performance and their statistical association with the predicted outcome, rather than direct neurophysiological causation. Further, given the small sample size and high-dimensional feature space, the findings should be considered exploratory and require validation in substantially larger and independent datasets.

To conclude, this work establishes a novel machine learning framework for predicting individualized TEP responses to iTBS and cTBSs. Approaches such as the one presented here are essential for enhancing the reliability, precision, and clinical adoption of TBS as a personalized therapeutic intervention for neurological and psychiatric disorders. To drive this innovation further, future studies should aim to validate these results in larger cross-dataset cohorts, explore the impact of EEG phase-specific (i.e., oscillatory phase-dependent) stimulation and individualized EEG-guided optimization of perturbation strength, refine modeling and further investigate the underlying neurophysiological mechanisms to enhance robustness and effectiveness.

CRediT authorship contribution statement

Arne Callaert: Writing – original draft, Software, Methodology, Investigation. **Kristl Vonck:** Writing – review & editing, Supervision, Conceptualization. **Diego Nieves Avendaño:** Writing – review & editing. **Sofie Carrette:** Resources, Data curation, Conceptualization. **Chiara Silvestri:** Writing – review & editing. **Philipp Schnepel:** Writing – review & editing, Funding acquisition. **Vojkan Mihajlović:** Writing – review & editing, Funding acquisition. **Evelien Carrette:** Writing – review & editing, Supervision, Conceptualization. **Femke Ongenae:** Writing – review & editing, Supervision, Conceptualization. **Sofie Van Hoecke:** Writing – review & editing, Supervision, Conceptualization.

Ethics statement

The study was conducted in accordance with the Declaration of Helsinki and approved by the institutional ethics committee of Ghent University Hospital (EC 2017/0780). The trial was registered at ClinicalTrials.gov (NCT05206162). All participants provided written informed consent prior to participation and were screened for contraindications to transcranial magnetic stimulation.

Funding

Part of this research is funded by imec.

Declaration of competing interest

Kristl Vonck has received free devices for research studies in normal volunteers and preclinical studies from LivaNova and Cerbomed. Kristl Vonck has received consultancy fees from LivaNova and Synergia Medical. Kristl Vonck has participated in advisory board meetings for LivaNova and Synergia Medical. Kristl Vonck also participated in advisory board meetings for Pharvaris and received consultancy fees from All Man Foundation, Angelini Pharma, Pharvaris, and Precisis. The remaining authors declare no commercial or financial relationships that could be construed as a potential conflict of interest.

Appendix A. Supplementary data

Supplementary material related to this article can be found online at https://doi.org/10.1016/j.neuroimage.2026.121957.

Data and code availability statement

The datasets generated and analyzed during the current study are not publicly available due to privacy and ethical restrictions. Requests for access to the data should be directed to Sofie Carrette (sofie.carrette@ugent.be). The code used for data preprocessing and analysis is available from the corresponding author upon reasonable request (arne.callaert@ugent.be).

References

Bertazzoli, G., Esposito, R., Mutanen, T.P., Ferrari, C., Ilmoniemi, R.J., Miniussi, C., Bortoletto, M., 2021. The impact of artifact removal approaches on TMS–EEG signal. NeuroImage 239, 118272.

Brancaccio, A., Tabarelli, D., Zazio, A., Bertazzoli, G., Metsomaa, J., Ziemann, U., Bortoletto, M., Belardinelli, P., 2024. Towards the definition of a standard in TMS-EEG data preprocessing. NeuroImage 301, 120874.

Cai, G., Xu, J., Ding, Q., Lin, T., Chen, H., Wu, M., Li, W., Chen, G., Xu, G., Lan, Y., 2024. Electroencephalography oscillations can predict the cortical response following theta burst stimulation. Brain Res. Bull. 208, 110902.

Carrette, S., Vonck, K., Klooster, D., Raedt, R., Carrette, E., Delbeke, J., Wadman, W., Casarotto, S., Massimini, M., Boon, P., 2025. Exploration of theta burst-induced modulation of transcranial magnetic stimulation-evoked potentials over the motor cortex. Neuromodulation: Technol. Neural Interface 28 (1), 123–135.

Casarotto, S., Fecchio, M., Rosanova, M., Varone, G., D'Ambrosio, S., Sarasso, S., Pigorini, A., Russo, S., Comanducci, A., Ilmoniemi, R.J., et al., 2022. The rt-TEP tool: real-time visualization of TMS-Evoked Potentials to maximize cortical activation and minimize artifacts. J. Neurosci. Methods 370, 109486.

Casarotto, S., Romero Lauro, L.J., Bellina, V., Casali, A.G., Rosanova, M., Pigorini, A., Defendi, S., Mariotti, M., Massimini, M., 2010. EEG responses to TMS are sensitive to changes in the perturbation parameters and repeatable over time. PLoS One 5 (4), e10281.

Chen, N.-F., Hassan, U., Ross, J.M., Forman, L., Hartford, J.W., Gogulski, J., Parmigiani, S., Truong, J., Keller, C.J., Cline, C.C., 2025. Noninvasive profiling of input-output excitability curves in human prefrontal cortex. BioRxiv.

Chung, S.W., Hill, A.T., Rogasch, N.C., Hoy, K.E., Fitzgerald, P.B., 2016. Use of theta-burst stimulation in changing excitability of motor cortex: a systematic review and meta-analysis. Neurosci. Biobehav. Rev. 63, 43–64.

Chung, S.W., Hoy, K.E., Fitzgerald, P.B., 2015. Theta-burst stimulation: A new form of TMS treatment for depression? Depress. Anxiety 32 (3), 182–192.

Cole, E., O'Sullivan, S.J., Tik, M., Williams, N.R., 2024. Accelerated theta burst stimulation: safety, efficacy, and future advancements. Biol. Psychiatry 95 (6), 523–535.

Conde, V., Tomasevic, L., Akopian, I., Stanek, K., Saturnino, G.B., Thielscher, A., Bergmann, T.O., Siebner, H.R., 2019. The non-transcranial TMS-evoked potential is an inherent source of ambiguity in TMS-EEG studies. NeuroImage 185, 300–312.

Delorme, A., Makeig, S., 2004. EEGLAB: an open-source toolbox for analysis of single-trial EEG dynamics including independent component analysis. J. Neurosci. Methods 134 (1), 9–21.

Desideri, D., Zrenner, C., Ziemann, U., Belardinelli, P., 2019. Phase of sensorimotor μ-oscillation modulates cortical responses to transcranial magnetic stimulation of the human motor cortex. J. Physiol. 597 (23), 5671–5686.

Dhami, P., Knyahnytska, Y., Atluri, S., Lee, J., Courtney, D.B., Croarkin, P.E., Blumberger, D.M., Daskalakis, Z.J., Farzan, F., 2019. Feasibility and clinical effects of theta burst stimulation in youth with major depressive disorders: an open-label trial. J. Affect. Disord. 258, 66–73.

Dhami, P., Moreno, S., Croarkin, P.E., Blumberger, D.M., Daskalakis, Z.J., Farzan, F., 2023. Baseline markers of cortical excitation and inhibition predict response to theta burst stimulation treatment for youth depression. Sci. Rep. 13 (1), 19115.

Donoghue, T., Haller, M., Peterson, E.J., Varma, P., Sebastian, P., Gao, R., Noto, T., Lara, A.H., Wallis, J.D., Knight, R.T., et al., 2020. Parameterizing neural power spectra into periodic and aperiodic components. Nature Neurosci. 23 (12), 1655–1665.

Farzan, F., Bortoletto, M., 2022. Identification and verification of a 'true' TMS evoked potential in TMS-EEG. J. Neurosci. Methods 378, 109651.

Fecchio, M., Pigorini, A., Comanducci, A., Sarasso, S., Casarotto, S., Premoli, I., Derchi, C.-C., Mazza, A., Russo, S., Resta, F., et al., 2017. The spectral features of EEG responses to transcranial magnetic stimulation of the primary motor cortex depend on the amplitude of the motor evoked potentials. PLoS One 12 (9), e0184910.

Gao, R., Peterson, E.J., Voytek, B., 2017. Inferring synaptic excitation/inhibition balance from field potentials. NeuroImage 158, 70–78.

Gramfort, A., Luessi, M., Larson, E., Engemann, D.A., Strohmeier, D., Brodbeck, C., Goj, R., Jas, M., Brooks, T., Parkkonen, L., et al., 2013. MEG and EEG data analysis with MNE-python. Front. Neuroinformatics 7, 267.

Guerra, A., López-Alonso, V., Cheeran, B., Suppa, A., 2020. Variability in non-invasive brain stimulation studies: Reasons and results. Neurosci. Lett. 719, 133330.

Hastie, T., Tibshirani, R., Wainwright, M., 2015. Statistical learning with sparsity. Monogr. Statist. Appl. Probab. 143 (143), 8.

Hernandez-Pavon, J.C., Veniero, D., Bergmann, T.O., Belardinelli, P., Bortoletto, M., Casarotto, S., Casula, E.P., Farzan, F., Fecchio, M., Julkunen, P., et al., 2023. TMS combined with EEG: Recommendations and open issues for data collection and analysis. Brain Stimul. 16 (2), 567–593.

Huang, Y.-Z., Edwards, M.J., Rounis, E., Bhatia, K.P., Rothwell, J.C., 2005. Theta burst stimulation of the human motor cortex. Neuron 45 (2), 201–206.

Huang, Y.-Z., Lu, M.-K., Antal, A., Classen, J., Nitsche, M., Ziemann, U., Ridding, M., Hamada, M., Ugawa, Y., Jaberzadeh, S., et al., 2017. Plasticity induced by non-invasive transcranial brain stimulation: a position paper. Clin. Neurophysiol. 128 (11), 2318–2329.

Katagiri, N., Saho, T., Shibukawa, S., Tanabe, S., Yamaguchi, T., 2024. Predicting interindividual response to theta burst stimulation in the lower limb motor cortex using machine learning. Front. Neurosci. 18, 1363860.

Kerwin, L.J., Keller, C.J., Wu, W., Narayan, M., Etkin, A., 2018. Test-retest reliability of transcranial magnetic stimulation EEG evoked potentials. Brain Stimul. 11 (3), 536–544.

Li, A., Feitelberg, J., Saini, A.P., Höchenberger, R., Scheltienne, M., 2022. MNE-ICALabel: Automatically annotating ICA components with ICLabel in python. J. Open Source Softw. 7 (76), 4484.

Lioumis, P., Kičić, D., Savolainen, P., Mäkelä, J.P., Kähkönen, S., 2009. Reproducibility of TMS—Evoked EEG responses. Hum. Brain Mapp. 30 (4), 1387–1396.

Lioumis, P., Rosanova, M., 2022. The role of neuronavigation in TMS–EEG studies: Current applications and future perspectives. J. Neurosci. Methods 380, 109677.

Makeig, S., Bell, A., Jung, T.-P., Sejnowski, T.J., 1995. Independent component analysis of electroencephalographic data. Adv. Neural Inf. Process. Syst. 8.

McCalley, D.M., Lench, D.H., Doolittle, J.D., Imperatore, J.P., Hoffman, M., Hanlon, C.A., 2021. Determining the optimal pulse number for theta burst induced change in cortical excitability. Sci. Rep. 11 (1), 8726.

Meisel, C., Plenz, D., Schulze-Bonhage, A., Reichmann, H., 2016. Quantifying antiepileptic drug effects using intrinsic excitability measures. Epilepsia 57 (11), e210–e215.

Meisel, C., Schulze-Bonhage, A., Freestone, D., Cook, M.J., Achermann, P., Plenz, D., 2015. Intrinsic excitability measures track antiepileptic drug action and uncover increasing/decreasing excitability over the wake/sleep cycle. Proc. Natl. Acad. Sci. 112 (47), 14694–14699.

Mutanen, T.P., Biabani, M., Sarvas, J., Ilmoniemi, R.J., Rogasch, N.C., 2020. Source-based artifact-rejection techniques available in TESA, an open-source TMS–EEG toolbox. Brain Stimul.: Basic Transl. Clin. Res. Neuromodulation 13 (5), 1349–1351.

Mutanen, T.P., Kukkonen, M., Nieminen, J.O., Stenroos, M., Sarvas, J., Ilmoniemi, R.J., 2016. Recovering TMS-evoked EEG responses masked by muscle artifacts. Neuroimage 139, 157–166.

Mutanen, T.P., Metsomaa, J., Liljander, S., Ilmoniemi, R.J., 2018. Automatic and robust noise suppression in EEG and MEG: The SOUND algorithm. Neuroimage 166, 135–151.

Ozdemir, R.A., Boucher, P., Fried, P.J., Momi, D., Jannati, A., Pascual-Leone, A., Santarnecchi, E., Shafi, M.M., 2021. Reproducibility of cortical response modulation induced by intermittent and continuous theta-burst stimulation of the human motor cortex. Brain Stimul. 14 (4), 949–964.

Pellegrino, G., Schuler, A.-L., Cai, Z., Marinazzo, D., Tecchio, F., Ricci, L., Tombini, M., Di Lazzaro, V., Assenza, G., 2024. Assessing cortical excitability with electroencephalography: A pilot study with EEG-iTBS. Brain Stimul. 17 (2), 176–183.

Premoli, I., Castellanos, N., Rivolta, D., Belardinelli, P., Bajo, R., Zipser, C., Espenhahn, S., Heidegger, T., Müller-Dahlhaus, F., Ziemann, U., 2014. TMS-EEG signatures of GABAergic neurotransmission in the human cortex. J. Neurosci. 34 (16), 5603–5612.

Prokhorenkova, L., Gusev, G., Vorobev, A., Dorogush, A.V., Gulin, A., 2018. CatBoost: unbiased boosting with categorical features. Adv. Neural Inf. Process. Syst. 31.

Rissanen, I.J., Granö, I., Souza, V.H., Sathyan, S., Thirugnanasambandam, N., Ilmoniemi, R.J., Lioumis, P., 2026. TMS–EEG indices to define local cortical excitability thresholds. BioRxiv, https://doi.org/10.64898/2026.01.12.699003.

Rocchi, L., Ibáñez, J., Benussi, A., Hannah, R., Rawji, V., Casula, E., Rothwell, J., 2018. Variability and predictors of response to continuous theta burst stimulation: a TMS-EEG study. Front. Neurosci. 12, 400.

Rogasch, N.C., Biabani, M., Mutanen, T.P., 2022. Designing and comparing cleaning pipelines for TMS-EEG data: A theoretical overview and practical example. J. Neurosci. Methods 371, 109494.

Rogasch, N.C., Fitzgerald, P.B., 2013. Assessing cortical network properties using TMS–EEG. Hum. Brain Mapp. 34 (7), 1652–1669.

Rogasch, N.C., Sullivan, C., Thomson, R.H., Rose, N.S., Bailey, N.W., Fitzgerald, P.B., Farzan, F., Hernandez-Pavon, J.C., 2017. Analysing concurrent transcranial magnetic stimulation and electroencephalographic data: A review and introduction to the open-source TESA software. Neuroimage 147, 934–951.

Sheen, J.Z., Mazza, F., Momi, D., Miron, J.-P., Mansouri, F., Russell, T., Zhou, R., Hyde, M., Fox, L., Voetterl, H., et al., 2024. N100 as a response prediction biomarker for accelerated 1 Hz right DLPFC-rTMS in major depression. J. Affect. Disord. 363, 174–181.

Speranza, B.E., Hill, A.T., Do, M., Cerins, A., Donaldson, P.H., Desarker, P., Oberman, L.M., Das, S., Enticott, P.G., Kirkovski, M., 2024. The neurophysiological effects of theta burst stimulation as measured by electroencephalography: A systematic review. Biol. Psychiatry: Cogn. Neurosci. Neuroimaging 9 (11), 1083–1120.

Suppa, A., Huang, Y.-Z., Funke, K., Ridding, M., Cheeran, B., Di Lazzaro, V., Ziemann, U., Rothwell, J., 2016. Ten years of theta burst stimulation in humans: established knowledge, unknowns and prospects. Brain Stimul. 9 (3), 323–335.

Terranova, C., Rizzo, V., Cacciola, A., Chillemi, G., Calamuneri, A., Milardi, D., Quartarone, A., 2019. Is there a future for non-invasive brain stimulation as a therapeutic tool? Front. Neurol. 9, 1146.

Tibshirani, R., 1996. Regression shrinkage and selection via the lasso. J. R. Stat. Soc. Ser. B Stat. Methodol. 58 (1), 267–288.

Wassermann, E., Epstein, C., Ziemann, U., Walsh, V., Paus, T., Lisanby, S., 2008. Oxford Handbook of Transcranial Stimulation. OUP Oxford.

Welch, P., 2003. The use of fast Fourier Transform for the estimation of power spectra: A method based on time averaging over short, modified periodograms. IEEE Trans. Audio Electroacoust. 15 (2), 70–73.

Wu, W., Keller, C.J., Rogasch, N.C., Longwell, P., Shpigel, E., Rolle, C.E., Etkin, A., 2018. ARTIST: A fully automated artifact rejection algorithm for single-pulse TMS-EEG data. Hum. Brain Mapp. 39 (4), 1607–1625.

Zhang, Y., Li, L., Bian, Y., Li, X., Xiao, Q., Qiu, M., Xiang, N., Xu, F., Wang, P., 2023. Theta-burst stimulation of TMS treatment for anxiety and depression: A FNIRS study. J. Affect. Disord. 325, 713–720.

Zhu, T., Cao, C., Coxon, J., Sack, A.T., Leunissen, I., 2024. Using TMS–EEG to study the intricate interplay between GABAergic inhibition and glutamatergic excitation during reactive and proactive motor inhibition. BioRxiv, https://doi.org/10.1101/2024.09.05.610957.